arXiv:0801.3737v1 [cond-mat.str-el] 24 Jan 2008

Raman scattering studies of temperature- and field-induced melting of charge order in (La,Pr,Ca)MnO_3

M. Kim,[1] H. Barath,[1] S.L. Cooper,[1] P. Abbamonte,[1] E. Fradkin,[1] M. Rübhausen,[2] C. L. Zhang,[3] and S-W. Cheong[3]

[1]*Department of Physics and Frederick Seitz Materials Research Laboratory, University of Illinois, Urbana, Illinois 61801*

[2]*Institut für Angewandte Physik, Universität Hamburg, Jungiusstraße 11, D-20355 Hamburg, Germany*

[3]*Rutgers Center for Emergent Materials and Department of Physics and Astronomy,*
Rutgers University, Piscataway, New Jersey 08854, USA

(Dated: February 5, 2008)

We present Raman scattering studies of the structural and magnetic phases that accompany temperature- and field-dependent melting of charge- and orbital-order (COO) in $La_{0.5}Ca_{0.5}MnO_3$ and $La_{0.25}Pr_{0.375}Ca_{0.375}MnO_3$. Our results show that thermal and field-induced COO melting in $La_{0.5}Ca_{0.5}MnO_3$ exhibits three stages in a heterogeneous melting process: at low temperatures and fields, we observe a long-range, strongly Jahn-Teller (JT) distorted/COO phase; at intermediate temperatures and/or fields, we find a coexistence regime comprising both strongly JT distorted/COO and weakly JT distorted/ferromagnetic metal (FMM) phases; and at high temperatures and/or high fields, we observe weakly JT distorted homogeneous paramagnetic (PM) or ferromagnetic (FM) phase. In the high field/high temperature regime of $La_{0.5}Ca_{0.5}MnO_3$ and $La_{0.25}Pr_{0.375}Ca_{0.375}MnO_3$, we identify a clear structural change to a weakly JT distorted phase that is associated with either a *Imma* or *Pnma* structure. We are able to provide a complete structural phase diagram of $La_{0.5}Ca_{0.5}MnO_3$ for the temperature and field ranges $6 \leq T \leq 170$ K and $0 \leq H \leq 9$ T. Significantly, we provide evidence that the field-induced melting transition of $La_{0.5}Ca_{0.5}MnO_3$ is first-order, and resembles a crystallization transition of an "electronic solid." We also investigate thermal and field-induced melting in $La_{0.25}Pr_{0.375}Ca_{0.375}MnO_3$ to elucidate the role of disorder in melting of COO. We find that while thermal melting of COO in $La_{0.25}Pr_{0.375}Ca_{0.375}MnO_3$ is quite similar to that in $La_{0.5}Ca_{0.5}MnO_3$, field-induced melting of COO in the two systems is quite different in several respects: the field-induced transition from the COO phase to the weakly JT-distorted/FM phase in $La_{0.25}Pr_{0.375}Ca_{0.375}MnO_3$ is very abrupt, and occurs at significantly lower fields ($H \sim 2$ T at $T \sim 0$ K) than in $La_{0.5}Ca_{0.5}MnO_3$ ($H \sim 30$ T at $T=0$ K); the intermediate coexistence regime is much narrower in $La_{0.25}Pr_{0.375}Ca_{0.375}MnO_3$ than in $La_{0.5}Ca_{0.5}MnO_3$; and the critical field H_c increases with increasing temperature in $La_{0.25}Pr_{0.375}Ca_{0.375}MnO_3$, in contrast to the decrease in H_c observed with increasing temperature in $La_{0.5}Ca_{0.5}MnO_3$. To explain these differences, we propose that field-induced melting of COO in $La_{0.25}Pr_{0.375}Ca_{0.375}MnO_3$ is best described as the field-induced percolation of FM domains, and we suggest that Griffiths phase physics may be an appropriate theoretical model for describing the unusual temperature- and field- dependent transitions observed in $La_{0.25}Pr_{0.375}Ca_{0.375}MnO_3$.

PACS numbers: 73.43.Nq, 75.47.Lx, 78.30.-j

I. INTRODUCTION

Strong phase competition in the manganese perovskites $A_{1-x}B_xMnO_3$ (A=trivalent rare earth, B=divalent alkaline earth) is known to spawn many of the interesting properties of these materials, such as their diverse phase behaviors as functions of temperature, rare earth ionic radius, doping, magnetic field, and pressure,[1,2,3,4,5,6,7,8,9,10,11] as well as the exotic phenomena these materials exhibit, including electronic phase separation,[12,13,14,15] colossal magnetoresistance,[16,17,18,19] and charge/orbital ordering (COO).[20,21,22] For example, $La_{0.5}Ca_{0.5}MnO_3$ exhibits a transition from a high temperature paramagnetic insulating (PI) phase to a ferromagnetic metal (FMM) phase at T_C=225 K, and then to a CE-type antiferromagnetic insulating (AFI) phase below T_N=155 K, in which the e_g orbitals on the Mn^{3+} sites alternate between $d_{3x^2-r^2}$ and $d_{3z^2-r^2}$ orbital configurations lying in the a-c plane (in the *Pnma* representation),[59] and the equal number of Mn^{3+} and Mn^{4+} ions form a checkerboard pattern on the lattice.[1,20,23,24,25] $La_{0.5}Ca_{0.5}MnO_3$ also exhibits significant structural changes associated with its electronic/magnetic phase transitions. At room temperature, the structure of $La_{0.5}Ca_{0.5}MnO_3$ is described by the space group *Pnma*.[24,26] However, below T_C there is evidence for the development of nanometer-scale phase regions with a superlattice structure having the space group $P2_1/m$, in which the unit cell is doubled along the a axis.[27] These $P2_1/m$ regions become more prominent with decreasing temperature below T_C, and eventually occupy the entire structure of $La_{0.5}Ca_{0.5}MnO_3$ below T_N.[28] There are also large changes in the lattice parameters between T_C and T_N in $La_{0.5}Ca_{0.5}MnO_3$: as the temperature decreases from T_C to T_N, the a axis increases by $\Delta a \sim 0.022$ Å, the c axis increases by $\Delta c \sim 0.041$ Å, and the b axis decreases by $\Delta b \sim -0.122$ Å.[20,23,24] This complex transition is associated with CE-type AFM charge/orbital order.[20,23,24] The zig-zag pattern of the COO configuration in $La_{0.5}Ca_{0.5}MnO_3$

(see Fig. 1(b))[20,21,22,23,24] is associated with cooperative JT distortions of the $Mn^{3+}O_6$ octahedra that lower the energy of those orbital states having lobes oriented along the long Mn-O octahedral bond directions. Accordingly, the polarization of orbitals in the a-c plane accounts for the decrease of the b axis—and the increase of the a and c axes—below T_N. The COO configuration in $La_{0.5}Ca_{0.5}MnO_3$ leads to an inequivalency of adjacent Mn sites below T_N, resulting in a doubling of the unit cell,[23,24,27,29,30] and favors CE-type AFM ordering, in which the spins *within* the zigzag chains are ferromagnetically ordered, while spins between adjacent chains are antiferromagnetically ordered. This magnetic ordering pattern is suggested by the semicovalent exchange coupling picture of Goodenough:[25] the singly semicovalent-bonded Mn^{3+}-O-Mn^{4+} structure along the chains favors FM coupling, while the doubly semicovalent-bonded Mn^{3+}-O-Mn^{3+}/Mn^{4+}-O-Mn^{4+} structure between the adjacent chains favors AFM coupling.[25]

A topic that continues to be of great interest in studies of COO in the manganites concerns the manner in which the COO state melts into disordered phases, either via classical thermal melting, or via quantum mechanical ($T\sim0$) melting. Temperature-dependent melting of COO in the manganites has been well-studied in a variety of measurements. For example, magnetic and transport measurements show that COO in $La_{0.5}Ca_{0.5}MnO_3$ melts into a FM metal phase above T_N, and that this transition is hysteretic—exhibiting an FM to AFM transition at T_N=135 K on cooling, and at T_N=180 K on warming—indicating that the thermally driven transition between AFM insulating and FM metal phases is first-order.[1] Electron and x-ray diffraction measurements of $La_{0.5}Ca_{0.5}MnO_3$ further show that the AFM to FM transition coincides with a transition from a commensurate (CM) to incommensurate (IC) charge-ordered phase, in which the COO superlattice peaks exhibit a decreased commensurability with the lattice and a suppression in intensity with increasing temperature up to T_{CO}=240K.[23,24,27] These results suggest that IC charge ordering coexists with the ferromagnetic metal phase in the temperature regime between T_N and T_{CO}. Electron microscopy studies also show that two-phase coexistence in $La_{0.5}Ca_{0.5}MnO_3$, $La_{5/8-y}Pr_yCa_{3/8}MnO_3$ (y=0.375, and 0.4), and $La_{0.33}Ca_{0.67}MnO_3$ originates from an inhomogeneous spatial mixture of FM and CO domains, whose sizes vary with temperature.[14,28,31] It was proposed that IC charge ordering results from thermal disordering of the e_g orbitals in the CO regions, which finally collapse completely at T_{CO}.[28] The same mechanism for thermal melting was also observed in electron diffraction and electron microscopy measurements of $La_{0.45}Ca_{0.55}MnO_3$ and $Pr_{0.5}Ca_{0.5}MnO_3$.[32]

In contrast to thermal melting of COO in the manganites, quantum mechanical (T=0) melting of COO in the manganites has been much less well studied, particularly using microscopic diffraction or spectroscopic probes. In quantum mechanical melting, the disruption of COO is induced near T=0 by tuning a control parameter such as doping, pressure, and magnetic field; consequently, quantum, rather than thermal, fluctuations may play a significant role in quantum melting of COO.[2,3,6,33,34] Most studies of quantum mechanical melting behavior have relied upon chemical substitution at the divalent cation site, but this method of phase tuning creates a disorder potential that is expected to have significant effects near quantum phase transitions.[1,6,7,13,34,35] While more limited in number, studies of magnetic-field-tuned melting of charge order in the manganites have been revelatory: Transport and magnetic studies of magnetic-field-tuned COO melting in $Nd_{0.5}Sr_{0.5}MnO_3$, $Pr_{0.5}Sr_{0.5}MnO_3$, and $Pr_{1-x}Ca_xMnO_3$ (x=0.3, 0.35, 0.4, and 0.5) showed that an applied magnetic field disrupts the AFM order associated with COO, and thereby disrupts the COO state, leading to a sharp drop in resistivity and a transition to a FM metal phase.[2,3,6,33] The hysteresis observed in these measurements indicates that the field-tuned AFM-to-FM transition is also a first order transition.[2,3,6,33] Optical measurements of $Pr_{0.6}Ca_{0.4}MnO_3$ and $Nd_{0.5}Sr_{0.5}MnO_3$ have also investigated the effects of thermal and field-induced melting of charge/orbital order on the optical spectral weight over a wide energy range.[33,36] However, while these bulk measurements have provided important information regarding the effects of thermal and field-induced melting on the physical properties of the manganites, they convey little information regarding the structural or other microscopic changes that accompany quantum melting of COO in the manganites.

Structural studies of COO field-induced melting in the manganites have been very limited. For example, field-dependent x-ray diffraction measurements of $La_{0.5}Ca_{0.5}MnO_3$, performed in the field range H=0 to 10 T, have been performed only at T=115 K, showing that the variance of the Mn-O-Mn bond length—and hence the size of the JT distortion—decreases with increasing field at this temperature.[37] However, there have been, as yet, no extensive structural studies of field-induced COO melting in the manganites over a more complete range of the H-T phase diagram.

The dearth of microscopic measurements of field- and pressure-tuned quantum phase transitions associated with COO in the manganites has left unanswered a variety of important questions, including: What microscopic changes accompany quantum mechanical melting of COO in the manganites as functions of pressure and magnetic field? Is there evidence in quantum phase transitions for novel phase behavior, such as electronic liquid crystal[38] or spin-glass phases? What magnetic and structural phases result when COO melts by tuning magnetic field or pressure? What is the role of disorder in the field- or pressure-tuned quantum phase transitions?

Field- and pressure-tuned inelastic light (Raman) scattering measurements provide a powerful method for studying structural and other microscopic details associated with quantum phase transitions in complex oxides.[39,40,41] For example, Raman scattering can provide energy, lifetime, and symmetry information about the important spin, charge, lattice, and orbital degrees-of-freedom in the manganites, and can convey important information regarding structural changes that accompany temperature- and field-dependent phase changes. Additionally, Raman measurements can be readily made under the 'extreme' conditions of low temperature, high magnetic field, and/or high pressure needed for studying quantum phase transitions in correlated materials.[39,40,41]

In this paper, we present temperature- and field-dependent Raman measurements of $\mathrm{La_{0.5}Ca_{0.5}MnO_3}$ and $\mathrm{La_{0.25}Pr_{0.375}Ca_{0.375}MnO_3}$, which enable us to map out the structural and COO phases of these materials in the temperature range 2–300 K and in the field range 0–9 T. Among the interesting results of these measurements: (i) We observe strong evidence that both field- and temperature-dependent melting of COO in $\mathrm{La_{0.5}Ca_{0.5}MnO_3}$ occurs in such a way as to preserve large coherent domains of COO throughout the melting process, indicating that field- and temperature-dependent melting in this material occurs primarily at the surfaces of COO regions. These results provide evidence that the field-induced melting transition of $\mathrm{La_{0.5}Ca_{0.5}MnO_3}$ is first-order, and resembles a crystallization transition of an "electronic solid." (ii) The similar effects of field- and temperature-dependent melting on the structure of $\mathrm{La_{0.5}Ca_{0.5}MnO_3}$ further suggests that magnetic fields and thermal disorder disrupt charge-ordering through a similar mechanism, i.e., by locally disordering AFM alignment. (iii) We observe the appearance of new modes in the high-field regimes of both $\mathrm{La_{0.5}Ca_{0.5}MnO_3}$ and $\mathrm{La_{0.25}Pr_{0.375}Ca_{0.375}MnO_3}$, which indicate that the melted high-field FM phase of these materials is associated with a structural phase having weakly JT distorted $\mathrm{MnO_6}$ octahedra. (iv) Finally, we find that substitution of Pr into $\mathrm{La_{1-x}Ca_xMnO_3}$—which allows us to study the effects of disorder on thermal and field-induced melting of the COO lattice—has dramatically different effects on thermal and field-induced COO melting. Specifically, we find that while thermal melting of COO into $\mathrm{La_{1-x}Ca_xMnO_3}$ is not dramatically affected by Pr-substitution, field-induced melting in $\mathrm{La_{0.25}Pr_{0.375}Ca_{0.375}MnO_3}$ is substantially more abrupt than that in $\mathrm{La_{0.5}Ca_{0.5}MnO_3}$. To explain this, we propose a Griffiths phase picture of COO melting in $\mathrm{La_{0.25}Pr_{0.375}Ca_{0.375}MnO_3}$ in which COO melting occurs via field-induced percolation of FM domains.

II. EXPERIMENTAL PROCEDURE

A. Sample details and preparation

Raman scattering measurements were performed on the as-grown surfaces of high-purity polycrystalline pellets of $\mathrm{La_{0.5}Ca_{0.5}MnO_3}$ (T_{CO}=240 K; Ref. 27) and $\mathrm{La_{0.25}Pr_{0.375}Ca_{0.375}MnO_3}$ (T_{CO}=210 K; Ref. 14). The pellets of both materials contained typical crystallite sizes between $3\times3\times3\mu\mathrm{m}^3$ and $5\times5\times5\mu\mathrm{m}^3$.

In the paramagnetic phase, $\mathrm{La_{0.5}Ca_{0.5}MnO_3}$ has an orthorhombic structure associated with the *Pnma* space group, which is isostructural to $\mathrm{LaMnO_3}$.[9,29,30] The *Pnma* structure is that of the simple cubic perovskite structure ($Pm\overline{3}m$ group symmetry), but with the $\mathrm{MnO_6}$ octahedra Jahn-Teller distorted and rotated along the [010] and [101] cubic axes. These changes give rise to the following values for the lattice parameters in $\mathrm{La_{0.5}Ca_{0.5}MnO_3}$: $a\approx b\approx\sqrt{2}a_c$ and $c\approx2a_c$, where a_c=the cubic perovskite lattice parameter.[29,30,42] Below T_N, x-ray and electron diffraction measurements indicate that the symmetry of $\mathrm{La_{0.5}Ca_{0.5}MnO_3}$ is lowered in the COO phase to a $P2_1/m$ structure, which involves a doubling of the *Pnma* unit cell to a structure with lattice parameters $a\approx2\sqrt{2}a_c$, $b\approx\sqrt{2}a_c$ and $c\approx2a_c$.[24,27]

B. Raman measurements

The Raman scattering measurements were performed using the 647.1 nm excitation line from a $\mathrm{Kr^+}$ laser. The incident laser power was limited to 10 mW, and was focused to a $\sim50\mu$m-diameter spot to minimize laser heating of the sample. The scattered light from the samples was collected in a backscattering geometry, dispersed through a triple stage spectrometer, and then detected with a liquid-nitrogen-cooled CCD detector. The incident light polarization was selected with a polarization rotator, and the scattered light polarization was analyzed with a linear polarizer, providing symmetry information about the excitations studied. The samples were inserted into a continuous He-flow cryostat, which was itself mounted in the bore of a superconducting magnet, allowing measurements in both the temperature range 4–350 K and the magnetic-field range 0–9 T.

C. Field measurements

Magnetic field measurements were performed in the Faraday ($\overrightarrow{q}\|\mathbf{H}$) geometry. To avoid Faraday rotation effects in applied magnetic fields, the incident light was circularly-polarized in the ($\mathbf{E}_i$, $\mathbf{E}_s$)=($\mathbf{L}$, $\mathbf{R}$) geometry,[60] where $\mathbf{E}_i$ and $\mathbf{E}_s$ are the incident and scattered electric field polarizations, respectively, and **L(R)** stands for left(right) circular polarization. This geometry allowed us to investigate modes with symmetries $A_g+B_{1g}+B_{2g}+B_{3g}$. The incident light was converted from linearly to circularly polarized light using a Berek compensator optimized for the 647.1 nm line, and the scattered light was converted back to linearly polarized light with a quarter-wave plate. In this paper, when listing the excitation symmetries observed, rather than referring to the $P2_1/m$ space group of the actual structure, we use the irreducible representations of the orthorhombic *Pmma* space group of the simplified structure in which the octahedral tilts

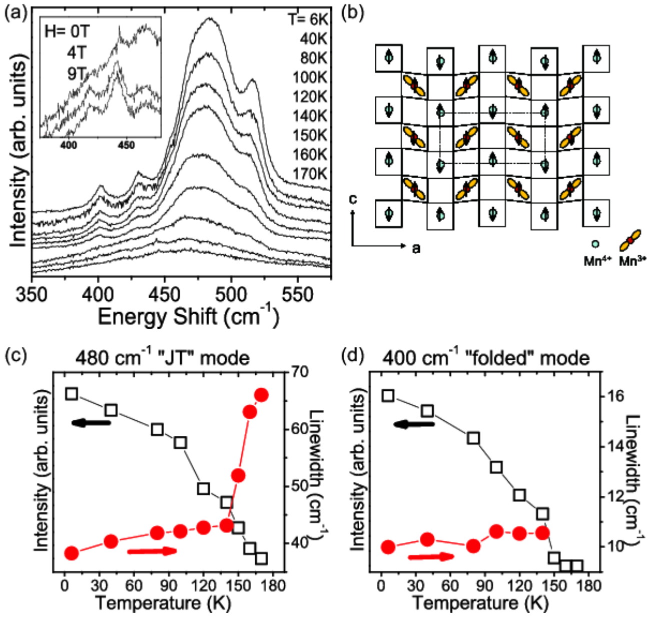

FIG. 1: (a) Temperature dependence of the Raman spectrum of $La_{0.5}Ca_{0.5}MnO_3$ in the temperature range 6–170 K. (inset) Field-dependence of the 420 cm^{-1} and 440 cm^{-1} "field-induced modes" for T=160 K, showing the enhancement of these modes with applied magnetic field. (b) Schematic representation of the *CE*-type AFM/charge/orbital order in $La_{0.5}Ca_{0.5}MnO_3$, showing the doubling of the unit cell. (c) Intensity (empty squares) and linewidth (filled circles) of the 480 cm^{-1} JT mode as a function of temperature. The intensity of this mode is suppressed by ∼85% from T=6 K to T=170 K. (d) Summary of the intensity (empty squares) and linewidth (filled circles) of the 400 cm^{-1} "folded phonon mode" as a function of temperature. The intensity of this mode is completely suppressed above T=150 K. The symbol sizes in parts (c) and (d) reflect an estimated 5% error associated with fits to the observed spectra.

(rotations) are not present, but in which the symmetry is lowered due to charge/orbital ordering. This simplification is justified[29] by the observation that the most intense Raman lines observed in $La_{0.5}Ca_{0.5}MnO_3$ are associated with those observed in the COO layered manganites.[43]

III. RESULTS AND DISCUSSION

A. Mode assignments

The temperature dependent Raman spectra of $La_{0.5}Ca_{0.5}MnO_3$ are shown in Figure 1(a). As the temperature is decreased below T_N=180 K, a broad peak near 465 cm^{-1} narrows, increases in intensity, and shifts to higher energies, attaining a value of roughly 480 cm^{-1} below T∼150 K. The evolution of this peak is concomitant with the growth of new peaks at 400, 430, and 515 cm^{-1} that appear in the COO phase. Notably, the temperature dependent Raman spectra we observe in Fig. 1(a) are consistent with those reported previously by Granado et al.,[44] Liarokapis et al.,[45] and Abrashev et al.[29] Also, a full symmetry analysis of the Raman spectra in both LL and LR geometries was previously reported in Naler et al.[34] In the following, we focus on the assignments of several phonon modes—including the 480 cm^{-1} phonon and newly observed modes at 400, 430, and 515 cm^{-1} in the COO phase—which are used in this study to monitor the field- and temperature-dependent evolution of various phases in $La_{0.5}Ca_{0.5}MnO_3$ and $La_{0.25}Pr_{0.375}Ca_{0.375}MnO_3$:

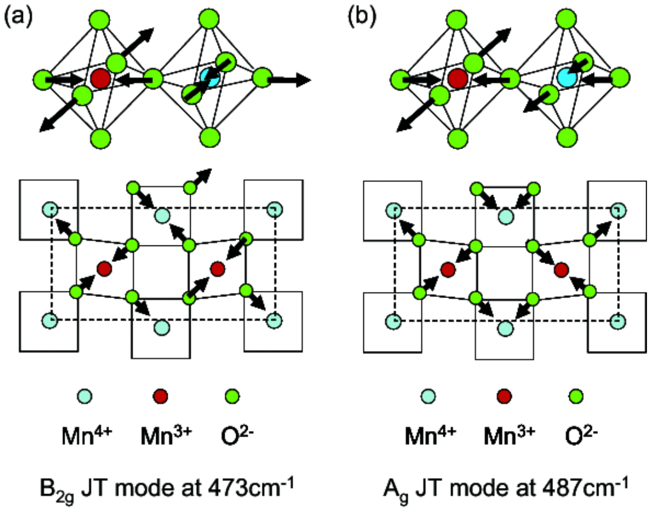
(a)
(b)
Mn^{4+}
Mn^{3+}
O^{2-}
Mn^{4+}
Mn^{3+}
O^{2-}
B$_{2g}$ JT mode at 473cm^{-1}
A$_g$ JT mode at 487cm^{-1}

FIG. 2: Normal modes associated with the 480 cm^{-1} JT peak: the 487 cm^{-1} B_{2g} and 473 cm^{-1} A_g asymmetric stretch modes of the oxygen atoms in the MnO_6 octahedra. (adapted from Ref. 29 and Ref. 43)

(i) *480 cm^{-1} "Jahn-Teller" mode* - The 480 cm^{-1} Jahn-Teller mode appears in both the LL and LR geometries.[34] Previous reports have attributed the 480 cm^{-1} peak to either Mn-O bending[29,42] or stretching[43,45,46] modes associated with the MnO_6 octahedra. We associate the 480 cm^{-1} peak with two nearly degenerate asymmetric Mn-O stretching modes of the MnO_6 octahedra (illustrated in Fig. 2), a B_{2g} mode at 473 cm^{-1} and an A_g mode at 487 cm^{-1}, based upon the following evidence: First, Raman studies show that the energy of the 480 cm^{-1} phonon is not sensitive to substitution at the rare-earth site, R.[46] This suggests that the 480 cm^{-1} phonon in $La_{0.5}Ca_{0.5}MnO_3$ is a Mn-O stretch mode, since substitution on the rare earth site R strongly affects the frequencies of the Mn-O bending modes.[61] Second, the broad band near 465 cm^{-1}—from which the 480 cm^{-1} phonon evolves—is activated in the Raman spectrum by JT distortions of the MnO_6 octahedra,[29,30,46,47] which lower the site symmetry and activate the asymmetric stretching modes. Consequently, the 480 cm^{-1} "Jahn-Teller" mode serves as an ideal probe of the degree to which JT distortions evolve through various temperature- and field-dependent transitions in

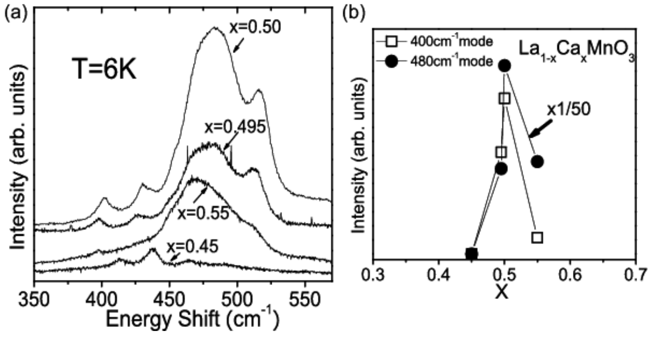

FIG. 3: (a) Doping dependence of the Raman spectrum of $La_{1-x}Ca_xMnO_3$ at x=0.5, 0.495, 0.55, and 0.45. (b) Summary of the intensity of the 400 cm^{-1} "folded phonon" mode (empty squares) and the 480 cm^{-1} JT mode (filled circles) as a function of doping.

$La_{0.5}Ca_{0.5}MnO_3$ and $La_{0.25}Pr_{0.375}Ca_{0.375}MnO_3$. The JT distortions of the MnO_6 octahedra are induced by the localization of e_g electrons on the Mn^{3+} sites, and consequently the presence of the 480 cm^{-1} mode can indicate even short-range charge/orbital order.

(ii) *"Folded phonon modes"* - The appearance of new peaks at 400, 430, and 515 cm^{-1} in the COO phase of $La_{0.5}Ca_{0.5}MnO_3$ below $T\sim150$ K (see Fig. 1(a)) reflects the doubling of the unit cell in the CO phase, which "folds" zone-boundary phonon modes to the zone center. Similar zone-folding behavior has been observed in the Raman spectra of other COO materials, including $La_{0.5}Sr_{1.5}MnO_4$ and $LaSr_2Mn_2O_7$.[43,62] The modes at 400 cm^{-1} and 430 cm^{-1} appear in both the LL and LR geometries, and the mode at 515 cm^{-1} appears in the LR geometry.[34] We attribute the new B_{2g} modes at 400 cm^{-1} and 430 cm^{-1}, and the A_g mode at 515 cm^{-1}, to Mn-O bending modes of the MnO_6 octahedra,[63] which become Raman-active in the monoclinic $P2_1/m$ structure that results from the doubling of the $Pnma$ phase by charge/orbital ordering.[29,30] Evidence for our interpretation is seen in the rapidity with which these modes disappear as $La_{1-x}Ca_xMnO_3$ is doped away from commensurate x=0.5 filling, as shown in Figure 3. The strong doping dependence of these 'activated' modes is indicative of the sensitivity of these folded modes to the loss of long-range charge and orbital order; consequently, we can use the intensities of these folded phonons to characterize the degree of long-range charge/orbital order in $La_{0.5}Ca_{0.5}MnO_3$ as functions of magnetic field and temperature.

(iii) *"Field-induced modes"* - Two modes at 420 cm^{-1} and 440 cm^{-1}, which are very weak but apparent in the zero-field spectrum at T=160 K, are dramatically enhanced with increasing magnetic field, as shown in the inset of Figure 1(a). These magnetic-field-induced modes are characteristic of spectra that have been observed for manganites having structural phases with weak or no JT distortions, i.e., with symmetric or nearly symmetric MnO_6 octahedra. These phases include rhombohedral $La_{0.67}Sr_{0.33}MnO_3$,[46] orthorhombic (FMM) $La_{0.67}Ca_{0.33}MnO_3$,[30,46,47] rhombohedral $La_{0.98}Mn_{0.96}O_3$,[30] and orthorhombic (PM) $CaMnO_3$.[48] Additionally, magnetic-field-dependent x-ray diffraction studies of $La_{0.5}Ca_{0.5}MnO_3$ provide further evidence that the MnO_6 octahedra have identical Mn-O bond lengths at high fields.[37] Therefore, we assume that the appearance of the new modes at 420 cm^{-1} and 440 cm^{-1} are indicative of a new structural phase that has no, or only weak, JT distortions.

Regarding the specific mode assignment of the 420 cm^{-1} and 440 cm^{-1} phonons, although it is unclear whether these modes are best associated with an orthorhombic $Pnma$ structure (of $LaMnO_3$) or with the rhombohedral structure,[30,47] there is a clear correspondence between the 420 cm^{-1} and 440 cm^{-1} field-induced modes of $La_{0.5}Ca_{0.5}MnO_3$ and the 465cm^{-1} and 487cm^{-1} modes in $CaMnO_3$;[48] the $\sim$46 cm^{-1} frequency difference between these pairs of modes can be attributed to the strong sensitivity of the frequency of these phonons to the R-O bond length reported by Martín-Carrón et al.[46] In $CaMnO_3$, the modes at 465 cm^{-1} and 487 cm^{-1} are activated by a $D_{[101]}$ type distortion, which involves a rotation (tilt) of the MnO_6 octahedra about the [101] cubic axis. This distortion is imposed on the cubic perovskite structure by the $Pm\overline{3}m$ symmetry, and results in a lowering of symmetry to the orthorhombic $Imma$ structure.[48] However, because $CaMnO_3$ also has both weak JT distortions and $D_{A-shift}$ type distortions of the MnO_6 octahedra, $CaMnO_3$ is most appropriately associated with the orthorhombic $Pnma$ structure.[48] The latter distortion involves a shift of the La/Ca atoms from their sites in the ideal perovskite in [100] direction (in the Pnma basis). Therefore, more study is needed to identify whether the specific structural phase we observe in $La_{0.5}Ca_{0.5}MnO_3$ at high magnetic fields is a $Pnma$ phase with weak JT distortions, or simply a $Imma$ phase with a $D_{[101]}$ basic distortion. In either case, we can use the field-induced modes at 420 cm^{-1} and 440 cm^{-1} to monitor the evolution of a "weakly JT distorted" ($Imma$ or $Pnma$) phase in $La_{0.5}Ca_{0.5}MnO_3$ and $La_{0.25}Pr_{0.375}Ca_{0.375}MnO_3$ as functions of magnetic field and temperature.

B. Raman studies of $La_{0.5}Ca_{0.5}MnO_3$

In the following, we describe the results of our temperature- and field-dependent Raman scattering measurements of $La_{0.5}Ca_{0.5}MnO_3$, in which material the COO state is fully commensurate and ordered (see Fig. 1(b)) at temperatures well below T_{CO}=240 K.

1. *Temperature dependence*

Fig. 1(a) shows that the four low temperature peaks at 480 cm^{-1}, 400 cm^{-1}, 430 cm^{-1}, and 515 cm^{-1} systematically lose intensity as a function of increasing temperature: the "folded phonon" peaks at 400 cm^{-1}, 430 cm^{-1}, and 515 cm^{-1} are completely suppressed above $T\sim150$ K, but exhibit very little change in linewidth throughout the temperature range 0–150 K. On the other hand, the 480 cm^{-1} "JT mode" persists above 150 K, but exhibits both a significant broadening in linewidth and a shift in energy above this temperature. The temperature dependent intensities and linewidths of the 480 cm^{-1} and 400 cm^{-1} modes are summarized in Figures 1(c) and 1(d). Fig. 1(a) also reveals that new weak peaks at 420 cm^{-1} and 440 cm^{-1} start to appear at $T\sim150$ K, above which temperature the folded phonon peaks are suppressed and the 480 cm^{-1} JT mode is weak but present. As shown in the inset of Fig. 1(a), the new peaks at 420 cm^{-1} and 440 cm^{-1} are very weak in the $H=0$ T spectra, but become significantly stronger with increasing magnetic field.

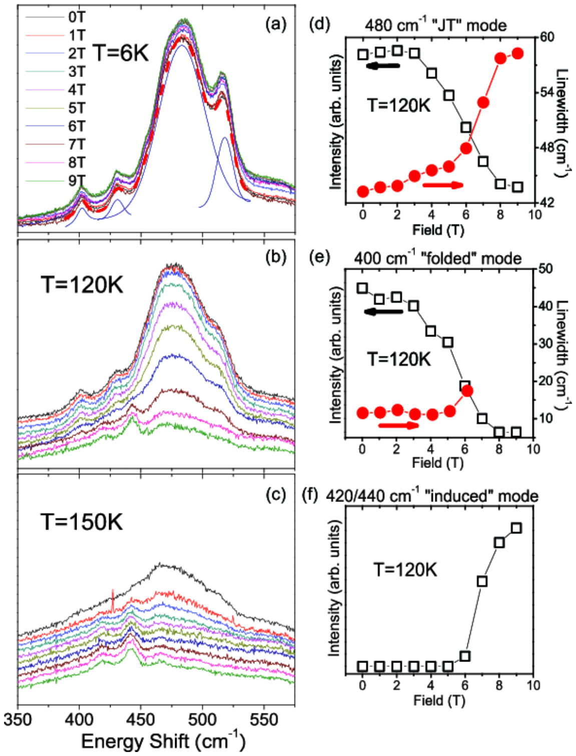

FIG. 4: (a) Magnetic field dependence of the Raman spectrum of $La_{0.5}Ca_{0.5}MnO_3$ at 6 K, illustrating the absence of a significant change in the spectrum with increasing magnetic field. The solid lines illustrate the examples of Gaussian and Lorentzian fits to the actual spectra, and the thick dashed line illustrates the sum of all individual fits. (b) Magnetic field dependence of the Raman spectrum of $La_{0.5}Ca_{0.5}MnO_3$ at 120 K, showing a significant suppression of the JT mode and the folded phonon modes, and indicating the appearance of field-induced modes near 420 cm^{-1} and 440 cm^{-1} with increasing magnetic field. (c) Magnetic field dependence of the Raman spectrum of $La_{0.5}Ca_{0.5}MnO_3$ at 150 K, showing the evolution of the 420 cm^{-1} and 440 cm^{-1} field-induced modes with increasing field. (d) Summary of the intensity (empty squares) and linewidth (filled circles) of the 480 cm^{-1} "JT mode" as a function of magnetic field. The intensity of this mode is suppressed by ∼80% from $H=0$ T to $H=9$ T. (e) Summary of the intensity (empty squares) and linewidth (filled circles) of the 400 cm^{-1} "folded phonon" mode as a function of magnetic field. The intensity of this mode is completely suppressed above $H=8$ T. (f) Summary of the combined intensities (empty squares) of the 420/440 cm^{-1} "field-induced phonon" modes as a function of magnetic field. The intensity of these modes is essentially fully developed above $H=8$ T. The symbol sizes in parts (d), (e), and (f) reflect an estimated 5% error associated with fits to the observed spectra.

2. *Field dependence*

Figs. 4(a), 4(b), and 4(c) show the field-dependent Raman spectra obtained at $T=6$ K, 120 K, and 150 K, respectively. Below $T=80$ K, Raman spectra taken as a function of magnetic field show little significant change in the linewidths or intensities of the modes between 0 T to 9 T, as shown in the spectra obtained at $T=6$ K in Fig. 4(a). However, for $T\geq80$ K, the intensities of the spectra become increasingly sensitive to the application of a magnetic field, as shown in the spectra obtained at $T=120$ K in Fig. 4(b). Figs. 4(d) and 4(e) summarize the field-dependent intensities and linewidths of both the 480 cm^{-1} "JT mode" and the 400 cm^{-1} "folded phonon mode" at $T=120$ K. The parameters of the 480 cm^{-1} "JT mode" were obtained from Gaussian fits and those of the 400 cm^{-1} "folded phonon mode" were obtained from Lorentzian fits to the spectra in Fig. 4, examples of which are illustrated by the solid curves in Fig. 4 (a).[64] The symbol sizes in Figs. 4(d) and (e) reflect the estimated 5% errors associated with these fits. The field-dependent development of both the intensities and linewidths of these peaks is very similar to their temperature-dependent evolution described earlier. In particular, while there are significant and systematic changes in the intensities of the "JT" and "folded phonon" modes with increasing field for $H<6$ T, there are much less dramatic changes in the linewidths of these modes with applied fields. However, the linewidths also show significant changes for 6 T$\leq H<8$ T. For $H\geq8$ T, the folded phonon mode disappears, but the 480 cm^{-1} JT mode persists with a residual intensity. The spectrum at $T=120$ K also illustrates that the new modes at 420 cm^{-1} and 440 cm^{-1} appear at $H\sim6$ T, indicating the appearance of a "weakly JT distorted" phase. These modes become enhanced with increasing field but show no significant enhancement For $H\geq8$ T, indicating a full development of the modes. The spectrum at $T=150$ K in Fig. 4(c) shows that the evolution of the "field-induced" modes occurs at a significantly lower magnetic field value $H^*(T)$ compared to that at $T=120$ K, and the modes are completely developed even at $H\sim3$ T. One also observes that, at T=150 K, the folded phonon modes are very weak at H=0 T, and disappear with even the smallest applied magnetic field, suggesting that long range COO is disrupted at this temperature even for small applied magnetic fields. We show the evolution of the folded phonon modes and the field-induced modes by plotting their intensities as functions of both magnetic field and temperature in Figs. 5(a) and 5(b).

3. Discussion

The temperature-dependent Raman spectra for $La_{0.5}Ca_{0.5}MnO_3$ allow us to draw several conclusions regarding the manner in which COO in $La_{0.5}Ca_{0.5}MnO_3$ melts with increasing temperature. First, the persistence with increasing temperature of the folded-phonon modes at 400, 430, and 515 cm^{-1}—which are again highly sensitive to the degree of long-range COO—suggest that long-range coherence of COO is preserved throughout much of the thermal melting process. This conclusion is also supported by the temperature dependence of the 480 cm^{-1} and 400 cm^{-1} mode linewidths: in the temperature regime well below the transition temperature (T<150 K in Fig. 1(c) and (d))—in which the size of the COO domain regions is much larger than the mean free path of the phonon—the 480 cm^{-1} and 400 cm^{-1} mode linewidths show no dependence on changing temperature. However, in the coexistence regime around the transition temperature (T>150 K in Fig. 1(c) and (d)), the 480cm^{-1} mode linewidth exhibits a rapid increase with temperature, indicating that the sizes of the COO domain regions have become smaller than the phonon mean free path. This temperature-dependent evolution is suggestive of a first-order "electronic crystallization" transition in $La_{0.5}Ca_{0.5}MnO_3$, in which the kinetics in the coexistence region corresponds to the propagation of a phase front. Indeed, our evidence that thermal melting in $La_{0.5}Ca_{0.5}MnO_3$ proceeds heterogeneously, by disrupting order at the surfaces of COO domain regions rather than by homogeneously disrupting COO domains, is consistent with TEM studies showing heterogeneous melting of COO in $La_{0.33}Ca_{0.67}MnO_3$.[31] Furthermore, the first-order nature of the COO melting transition in three-dimensional (3D) $La_{0.5}Ca_{0.5}MnO_3$ is also supported by the fact that this transition differs substantially from the continuous (second-order) CDW transition in layered (quasi-2D) dichalcogenides such as 1T-$TiSe_2$: in the latter system, there is roughly a five-fold increase in the linewidth of the CDW amplitude modes with increasing temperature or pressure, suggesting a very rapid—and roughly uniform—dissolution of long-range CDW order throughout the melting process.[40] It is interesting to note that the observed differences in the ordering transitions of 3D $La_{0.5}Ca_{0.5}MnO_3$ and quasi-2D 1T-$TiSe_2$ are also consistent with theoretical calculations of ordering behavior in 3D and 2D systems: variational renormalization group calculations of the three-dimensional three-state Potts model—which is an appropriate description of the three-fold degeneracy associated with ordering in cubic $La_{0.5}Ca_{0.5}MnO_3$—predict that the ordering transition should be weakly first order.[49,50] The addition of lattice degrees of freedom (i.e., a compressible system) has been shown to further "harden" the first-order nature of the transition in 3D systems.[51,52] On the other hand, calculations of the two-dimensional three-state Potts model—which is appropriate for layered dichalcogenides such as 1T-$TiSe_2$ because of the three commensurate CDWs in these quasi-2D materials—predict that the ordering transition should be continuous.[49] We note, however, that the presence of a critical amount of disorder in 3D systems is expected to round the first order transition and make the transition difficult to distinguish from a continuous phase transition.[53,54]

Our results allow us to identify several distinct electronic and structural phases in cubic $La_{0.5}Ca_{0.5}MnO_3$ as a function of temperature: (i) *Long-range COO regime* - Below 150 K, long-range COO persists in $La_{0.5}Ca_{0.5}MnO_3$, as suggested by the presence of folded phonons and by the temperature-insensitive linewidths of the 480 cm^{-1} JT mode. (ii) *Short-range COO regime* - In the temperature range 150–170 K, long-range coherence of COO in $La_{0.5}Ca_{0.5}MnO_3$ becomes suppressed—as evidenced in this temperature regime by the persistence of a 480 cm^{-1} JT mode with a significantly broadened linewidth, and by the disappearance of the folded phonon modes—indicating a phase regime in which short-range COO prevails. The appearance of new modes at 420 cm^{-1} and 440 cm^{-1} in this temperature range, $150 \leq T \leq 170$ K, also indicates that "weakly JT distorted" phase regions coexist with the strongly JT distorted COO regions in this regime. (iii) *Weakly JT distorted regime* - At very high temperatures (T>200 K), the 480 cm^{-1} JT mode is almost completely suppressed, and the 420 cm^{-1} and 440 cm^{-1} modes are clearly evident, indicating the presence of a weakly JT-distorted FMM regime associated with either a $Imma$ or $Pnma$ phase in this temperature range.

These results suggest the following description of the thermal melting process in $La_{0.5}Ca_{0.5}MnO_3$: With increasing temperature below 150 K, first-order melting primarily proceeds at the interface between large coherent COO regions, thereby shrinking the COO volume, but maintaining long-range coherence of COO domains; at still higher temperatures ($150 \leq T \leq 170$ K), additional melting leads to the eventual collapse of long-range COO, and the development of a regime in which short-range COO coexists with a "weakly JT distorted" phase. This melting process is consistent with the thermal melting of COO observed in earlier studies of $La_{0.5}Ca_{0.5}MnO_3$, in which a commensurate (CM) charge/orbital ordered phase was observed to melt with increasing temperature into an incommensurate (IC) charge ordering regime that coexists with the ferromagnetic metal phase above T_N=180K.[23,24,27] In fact, the high temperature modes we observe at 420 cm^{-1} and 440 cm^{-1}, which are indicative of the weakly JT distorted phase, are known to be associated with the Raman spectrum of ferromagnetic metallic $La_{0.55}Ca_{0.45}MnO_3$ shown in Figure 3(a). Our description of the thermal melting process in $La_{0.5}Ca_{0.5}MnO_3$ is also consistent with the three-step "heterogeneous" formation process of charge ordering (CO) observed by Tao and Zuo in $La_{0.33}Ca_{0.67}MnO_3$ using transmission electron microscopy (TEM):[31] short-range CO in $La_{0.33}Ca_{0.67}MnO_3$ initially forms at T∼280K; CO regions then grow with decreasing temperature via cluster formation; and finally, long-range CM CO develops via the percolation of these clusters below $T\sim235$K.[31] Because Raman scattering is a q=0 probe, we are not able to estimate the size of the CO domains. However, previous electron microscopy studies have estimated their size to be approximately 10-20 nm at 200 K and 50-60 nm at 125 K.[28]

Interestingly, our field-dependent Raman results in $La_{0.5}Ca_{0.5}MnO_3$ (see Sec. III B 2) indicate a strong similarity between the thermal and field-induced disruption of COO in this material. For example, the persistence of the folded phonon modes—as well as the insensitivity of the 480 cm^{-1} and 400 cm^{-1} mode linewidths—with increasing magnetic field below 6 T at T=120 K suggests that domains characterized by long-range COO persist throughout much of the field-induced melting process. Second, the appearance of new field-induced modes, and the persistence of the 480 cm^{-1} JT mode above 6 T at T=120 K, are indicative of the coexistence in this high field range of a weakly JT distorted/FMM phase (associated with either a *Imma* or *Pnma* structure; see Sec. III Aiii) and a short-range COO phase.

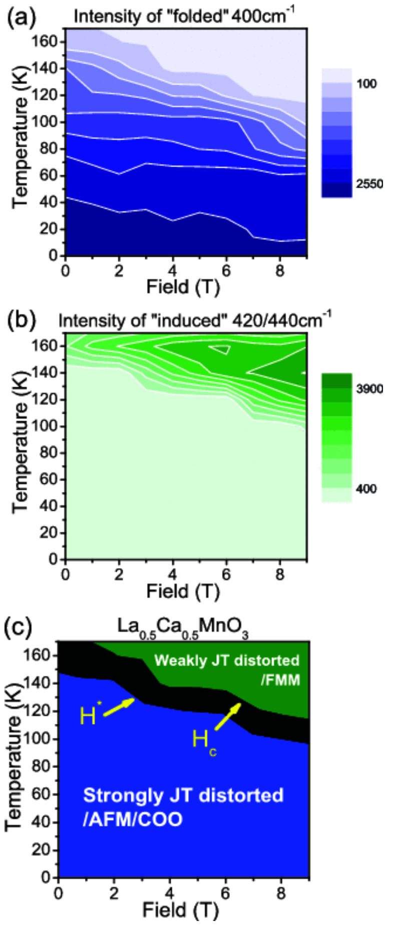

FIG. 5: (a) Contour plot of the intensity of the 400 cm^{-1} folded phonon mode as functions of temperature and magnetic field. The dark (purple) shades indicate the prevalence of the strongly JT distorted ($P2_1/m$ space group) structural phase, which is associated with the AFM/COO phase. (b) Contour plot of the combined intensities of the 420 cm^{-1} and 440 cm^{-1} field-induced modes as functions of temperature and field. The dark (green) shades indicate the prevalence of the weakly JT distorted (*Imma* or *Pnma* space group) structural phase, which is associated with the ferromagnetic metal (FMM) phase. (c) Temperature/magnetic field phase diagram of $La_{0.5}Ca_{0.5}MnO_3$ inferred from the intensity plots in (a) and (b), showing the phase boundary, $H^*(T)$, between the strongly JT distorted ($P2_1/m$ space group) AFM/COO phase (purple) and intermediate "coexistence" phase (black) regimes, and the phase boundary, $H_c(T)$, between the intermediate "coexistence" phase (black) and weakly JT distorted (*Imma* or *Pnma* space group) FMM phase (green) regimes.

The similarities between thermal and field-induced melting of COO in $La_{0.5}Ca_{0.5}MnO_3$ suggest that the application of a magnetic field also disrupts antiferromagnetic order preferentially at the surface of COO regions, giving rise to heterogeneous melting of the coherent long-range COO regions, and the evolution of a field regime in which short-range COO regions coexist with weakly JT distorted/FMM regions. Notably, our field-dependent Raman results suggest a three-stage field-dependent melting process in $La_{0.5}Ca_{0.5}MnO_3$, consistent with the three distinct structural phases identified by Tyson et al.[37] in field-dependent x-ray absorption measurements at T=115 K. Indeed, although the structural details inferred by the x-ray measurements were obtained only at T=115 K,[37] the comparisons of these x-ray results to our more extensive temperature- and field-dependent Raman measurements suggest that one can generalize the following structural details throughout H-T phase diagram: (i) *Low field-regime* - At low magnetic fields (e.g., $0\leq H\leq6$ T at T=120 K), only the 480 cm^{-1} "JT mode" and the 400 cm^{-1} "folded phonon" modes are present, indicative of a long-range "strongly JT distorted"/COO phase. X-ray absorption measurements (at T=115 K) confirm that the distribution of Mn-O and Mn-Mn separations exhibit only a weak field dependence in this regime.[37] (ii) *High field regime* - Above a critical field value $H_c(T)$ (e.g., $H_c\sim7$ T at T=120 K), the 400 cm^{-1} folded phonon mode is completely suppressed, and the field-induced 420 and 440 cm^{-1} modes are fully developed, indicative of a long-range "weakly JT distorted"/FMM phase associated with either a *Imma* or a *Pnma* structure. Field-dependent x-ray data at T=115 K indicate that the transformation to this high-field FM regime is accompanied, first, by a reduction of the Debye-Waller (DW) factor for the Mn-O distribution to $\sigma^2\sim0.0032$, which is comparable to that of $CaMnO_3$, and second, by the development of a Gaussian radial Mn-O distribution, indicating the disappearance of JT distortions. The average Mn-O bond distance also approaches a value of 1.96 Å in the high-field FM region, which corresponds to the average Mn-O bond distance found in FM $La_{1-x}Ca_xMnO_3$ near x=0.33.[37] (iii) *Intermediate field regime* - In the intermediate field range (e.g., 6≤H≤7 T at T=120 K), the folded phonons are very weak, and the 420 and 440 cm^{-1} modes start to appear, indicative of a coexistent phase regime with a combination of strongly JT distorted/COO and weakly JT distorted/FMM phase regions. A narrow mixed-phase region was also observed at intermediate field-values by x-ray absorption measurements.[37] The similarity between thermal and field-induced melting behavior of the 480 cm^{-1} "JT mode" in $La_{0.5}Ca_{0.5}MnO_3$ suggests that—like the T-dependent phase transition—the field-induced COO transition is a first-order quantum phase transition associated with melting of an electronic "crystal," and that the "intermediate field regime" can be identified with the coexistence phase regime in which the phonon mean free path is on the order of, or longer than, the size of the COO domain regions.

The three phase regimes implied by our Raman results are summarized in the magnetic-field- and temperature-dependent phase diagram of $La_{0.5}Ca_{0.5}MnO_3$, shown in Figure 5(c), obtained by combining the intensity plots of the folded phonon (Fig. 5(a)) and field-induced (Fig. 5(b)) modes. The resulting structural H-T phase diagram is indicative of a very robust COO state in $La_{0.5}Ca_{0.5}MnO_3$, with critical field values, $H^*(T)$—between the long-range COO and intermediate "coexistence" regimes—and $H_c(T)$—between the intermediate "coexistence" and weakly JT distorted FMM regimes—that decrease roughly linearly with decreasing temperature at a rate of ∼−0.2 T/K. Extrapolating this first-order critical field line to higher field values suggests an approximate T=0 critical point of $H^*(T=0)\sim 30$ T for $La_{0.5}Ca_{0.5}MnO_3$.

C. Raman studies of $La_{0.25}Pr_{0.375}Ca_{0.375}MnO_3$

It is of interest to explore the effects of disorder on thermal and field-induced melting of the robust COO state observed $La_{0.5}Ca_{0.5}MnO_3$, in order to explore the manner in which disorder destabilizes COO in the maganites. The effects of disorder on commensurate COO in $La_{0.5}Ca_{0.5}MnO_3$ can be investigated by substituting Pr in the $La_{1-x}Ca_xMnO_3$ lattice. The random substitution by Pr ions having a 3+ valence state results in the deviation from a commensurate composition x=0.5, but preserves the COO state even at the DE (double exchange)-optimized composition x=0.375, due to the relatively small ionic size of Pr.[14] Accordingly, Pr-substitution into commensurate $La_{0.5}Ca_{0.5}MnO_3$ has the effect of disordering the commensurate charge-ordered lattice, as schematically illustrated in Fig. 6(b). In the following, we describe the results of temperature- and field-dependent Raman scattering measurements of $La_{0.25}Pr_{0.375}Ca_{0.375}MnO_3$, in which we investigate the effects of disorder on temperature- and field-induced melting of COO.

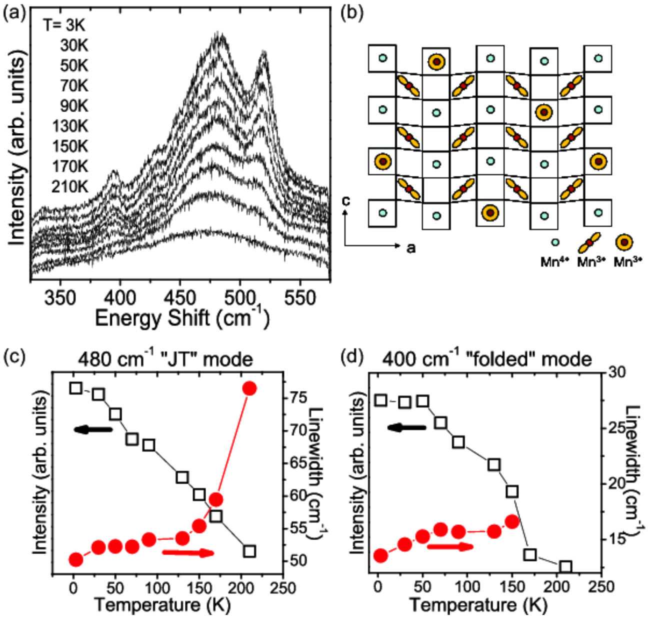

FIG. 6: (a) Temperature dependence of the Raman spectrum of $La_{0.25}Pr_{0.375}Ca_{0.375}MnO_3$ in the temperature range 3.5–210 K. (b) Schematic representation of the effect of Pr-substitution in $La_{0.25}Pr_{0.375}Ca_{0.375}MnO_3$ on COO, where double circles represent charge (hole) defects in COO. (c) Summary of the intensity (empty squares) and linewidth (filled circles) of the 480 cm^{-1} "JT mode" of $La_{0.25}Pr_{0.375}Ca_{0.375}MnO_3$ as a function of temperature. The intensity of this mode is suppress by ∼75% from T=3.5 K to T=210 K. (d) Summary of the intensity (empty squares) and linewidth (filled circles) of the 400 cm^{-1} "folded phonon" mode of $La_{0.25}Pr_{0.375}Ca_{0.375}MnO_3$ as a function of temperature. The intensity of this mode is completely suppressed above T=170 T. The symbol sizes in parts (c) and (d) reflect an estimated 5% error associated with fits to the observed spectra.

1. *Temperature dependence*

The temperature dependent Raman spectra of $La_{0.25}Pr_{0.375}Ca_{0.375}MnO_3$ are shown in Figure 6(a). Note that the temperature dependence of the Raman spectra in the COO phase of $La_{0.25}Pr_{0.375}Ca_{0.375}MnO_3$ is not significantly different from that of $La_{0.5}Ca_{0.5}MnO_3$: The "folded modes" at 400, 430, and 520 cm^{-1} gradually lose intensity with relatively little change in linewidth, eventually becoming suppressed above $T\sim$170 K; however, the 480cm^{-1} mode persists above $T\sim$170K, similar to the temperature-dependent behavior observed in $La_{0.5}Ca_{0.5}MnO_3$. The remark-

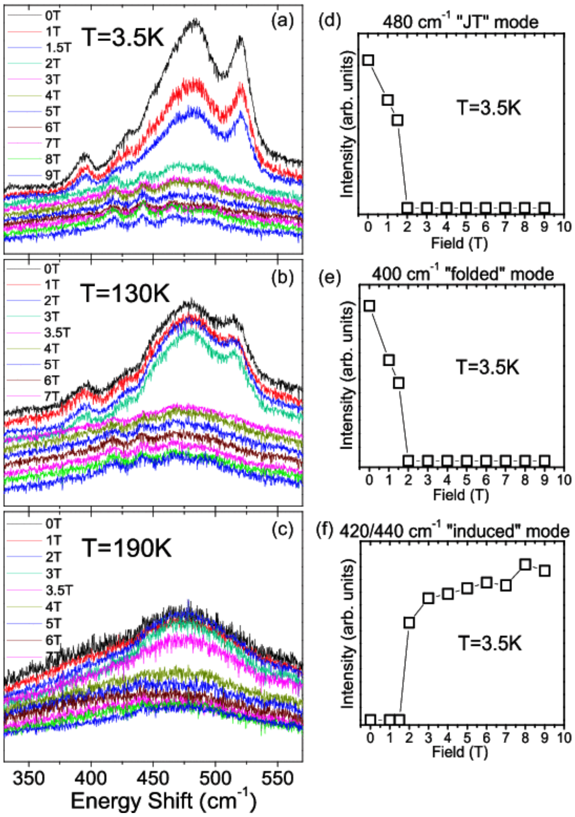

FIG. 7: (a) Magnetic field dependence of the Raman spectrum of $La_{0.25}Pr_{0.375}Ca_{0.375}MnO_3$ at 3.5 K, showing a dramatic suppression of the 480 cm^{-1} JT and 400 cm^{-1} folded phonon modes, and the appearance of the 420 cm^{-1} and 440 cm^{-1} field-induced modes at $H \sim 2$ T. (b) Magnetic field dependence of the Raman spectrum of $La_{0.25}Pr_{0.375}Ca_{0.375}MnO_3$ at 130 K, showing an abrupt field-induced transition between strongly JT distorted and weakly JT distorted structural phases. (c) Magnetic field dependence of the Raman spectrum of $La_{0.25}Pr_{0.375}Ca_{0.375}MnO_3$ at 190 K. (d) Summary of the intensity (empty squares) and linewidth (filled circles) of the 480 cm^{-1} "JT mode" as a function of magnetic field. The intensity of this mode is completely suppressed above H=2 T. (e) Summary of the intensity (empty squares) and linewidth (filled circles) of the 400 cm^{-1} "folded phonon" mode as a function of magnetic field. The intensity of this mode is completely suppressed above H=2 T. (f) Summary of the combined intensities (empty squares) of the 420/440 cm^{-1} "field-induced phonon" modes as a function of magnetic field. The intensity of this mode is essentially fully developed above H=2 T. The symbol sizes in parts (d), (e), and (f) reflect an estimated 5% error associated with fits to the observed spectra.

able similarity between the temperature dependences of the $La_{0.25}Pr_{0.375}Ca_{0.375}MnO_3$ and $La_{0.5}Ca_{0.5}MnO_3$ Raman spectra suggest that disordering COO with Pr-substitution does not appreciably affect temperature-dependent melting of COO in this material.

2. *Field dependence*

In contrast with the temperature-dependent evolution of the Raman spectrum in $La_{0.25}Pr_{0.375}Ca_{0.375}MnO_3$, the field-dependent evolution of the $La_{0.25}Pr_{0.375}Ca_{0.375}MnO_3$ spectrum differs markedly from that observed in $La_{0.5}Ca_{0.5}MnO_3$, as illustrated in Figs. 7. Specifically, even in the lowest temperature spectrum measured at $T \sim 3.5$ K, shown in Fig 7(a), the 480 cm^{-1} "JT mode" and the 400 cm^{-1} "folded phonon mode" of $La_{0.25}Pr_{0.375}Ca_{0.375}MnO_3$ exhibit a dramatic and abrupt decrease in intensity with increasing magnetic field, becoming suppressed above a critical field of roughly $H_c \sim 2$ T. Furthermore, above this critical field, there is an abrupt appearance of the field-induced 420 and 440 cm^{-1} modes, signaling the appearance of a "weakly JT" distorted phase. This strong field dependence is in strong contrast to the field-independence observed in $La_{0.5}Ca_{0.5}MnO_3$ for T<80 K. Additionally, this strong field dependence is different than the field dependence of $La_{0.5}Ca_{0.5}MnO_3$ observed even in high temperatures T>80 K. Specifically, $La_{0.5}Ca_{0.5}MnO_3$ exhibits a gradual change in intensities of all the modes with increasing field, as well as an intermediate field regime in which both the folded phonon modes and weakly JT distorted modes are observed, indicating the coexistence of long-range COO and weakly JT distorted regions in this field range. By contrast, the field dependence observed at T=3.5 K in $La_{0.25}Pr_{0.375}Ca_{0.375}MnO_3$ is much more dramatic, exhibiting an abrupt change in the spectrum between 1.5 and 2 T without any evidence for an intermediate field regime characterized by phase coexistence. Interestingly, the abrupt change in the spectrum is even more remarkable at higher temperatures, as illustrated by the field dependent data at T=130 K shown in Fig. 7(b) and T=190 K shown in Fig. 7(c): Specifically, at T=130 K, the "low-field regime" spectrum shows no field dependence up to $H \sim 3$ T. However, there is a striking transition to the "weakly JT distorted" spectral response between 3 and 3.5 T. At T=190 K, such a dramatic transition occurs between 3.5 and 4 T, again with no evidence for an intermediate field regime characterized by phase coexistence. Above the critical field, the "weakly JT distorted" spectrum shows no additional field dependence; that is, this field-induced transition in $La_{0.25}Pr_{0.375}Ca_{0.375}MnO_3$ appears to be an abrupt and direct change from the COO/AFM phase to the weakly JT distorted/FM phase.

Figure 8(a) and 8(b) illustrate the field dependence of the intensities of the 400 cm^{-1} "folded phonon" and the 420 and 440 cm^{-1} field-induced modes in $La_{0.25}Pr_{0.375}Ca_{0.375}MnO_3$ in the temperature range 3.5–210 K. These intensity plots enable us to map out a structural and COO phase diagram for $La_{0.25}Pr_{0.375}Ca_{0.375}MnO_3$ in the temperature range 3.5–210 K and in the field range 0–9 T. Interestingly, unlike $La_{0.5}Ca_{0.5}MnO_3$, the critical field

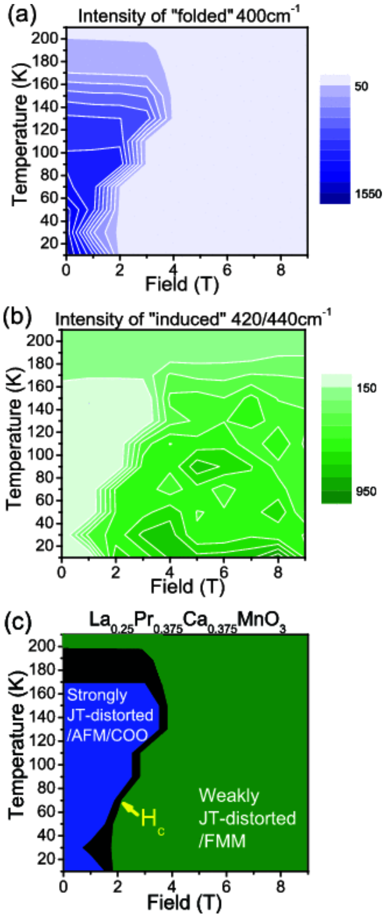

FIG. 8: (a) Contour plot of the intensity of the 400 cm^{-1} folded phonon mode in $La_{0.25}Pr_{0.375}Ca_{0.375}MnO_3$ as functions of temperature and field. The dark (purple) shades indicate the prevalence of the strongly JT distorted ($P2_1/m$ space group) structural phase, which is associated with the AFM/COO phase. (b) Contour plot of the combined intensities of the 420 and 440 cm^{-1} field-induced modes of $La_{0.25}Pr_{0.375}Ca_{0.375}MnO_3$ as functions of temperature and field. The dark (green) shades indicate the prevalence of the weakly JT distorted ($Imma$ or $Pnma$ space group) structural phase, which is associated with the ferromagnetic metal (FMM) phase. (c) Temperature/magnetic field phase diagram of $La_{0.25}Pr_{0.375}Ca_{0.375}MnO_3$, inferred from the intensity plots in (a) and (b), illustrating strongly JT distorted ($P2_1/m$ space group) AFM/COO phase (purple), weakly JT distorted ($Imma$ or $Pnma$ space group) FMM phase (green), and coexistent crossover phase (black) regimes.

H_c between strongly JT distorted/COO and weakly JT distorted/FMM phases in $La_{0.25}Pr_{0.375}Ca_{0.375}MnO_3$ doesn't show a monotonic decrease as a function of increasing temperature, but rather increases systematically from ~2 T to 4 T with increasing temperature.

3. *Discussion*

Field-induced and thermal melting of COO in $La_{0.25}Pr_{0.375}Ca_{0.375}MnO_3$ exhibit two noteworthy differences compared with melting of COO in $La_{0.5}Ca_{0.5}MnO_3$: (i) Pr-substitution causes a remarkable disparity between field-induced and thermal melting of COO in $La_{0.25}Pr_{0.375}Ca_{0.375}MnO_3$ that is not observed in $La_{0.5}Ca_{0.5}MnO_3$; more specifically, thermal melting of COO in $La_{0.25}Pr_{0.375}Ca_{0.375}MnO_3$ shows little difference from that observed in $La_{0.5}Ca_{0.5}MnO_3$, but field-induced melting of COO in $La_{0.25}Pr_{0.375}Ca_{0.375}MnO_3$ is substantially more abrupt—and occurs at significantly lower fields—than field-induced melting of COO in $La_{0.5}Ca_{0.5}MnO_3$; and (ii) Pr-substitution causes a dramatic reduction in the size of the coexistent phase regime (black regions in Figs. 5(c) and 8(c)) in the HT-structural phase diagram compared to that observed in $La_{0.5}Ca_{0.5}MnO_3$. This leads to a significantly more abrupt field-induced transition in $La_{0.25}Pr_{0.375}Ca_{0.375}MnO_3$ between the strongly JT distorted ($P2_1/m$ space group) AFM/COO phase (purple region in Fig. 8(c)) and weakly JT distorted ($Imma$ or $Pnma$ space group) FMM phase (green region in Fig. 8(c)).

To explain this behavior, we note first that earlier work on $La_{0.25}Pr_{0.375}Ca_{0.375}MnO_3$ by Uehara et al. reported the coexistence of long-range FM domains and long-range COO domains for $T<80$ K and $H=0$ T, and the coexistence of short-range COO domains and short-range FM domains for 80<T<210 K and $H=0$ T.[14] Accordingly, the dramatic difference between thermal and field-induced melting we observe in $La_{0.25}Pr_{0.375}Ca_{0.375}MnO_3$ indicates that—by favoring FM domains at the expense of COO domains—applied magnetic fields are far more effective than thermal fluctuations at disrupting long-range coherence between COO domains and driving a COO/AFM to FM transition, in $La_{0.25}Pr_{0.375}Ca_{0.375}MnO_3$. This description is consistent with the observed increase with temperature in the critical field $H_c(T)$ at which $La_{0.25}Pr_{0.375}Ca_{0.375}MnO_3$ transitions from the COO/AFM regime to the weakly JT distorted FM regime (see Fig. 8(c)): with increasing temperature, the size of the FM domains in $La_{0.25}Pr_{0.375}Ca_{0.375}MnO_3$ is known to decrease to nanometer length scales,[14] thereby creating more PM regions and a higher critical field needed to achieve a percolation transition of the FM domains in the FM "weakly JT distorted" phase. Thus, we argue that field-induced melting of long-range COO is fundamentally different in $La_{0.25}Pr_{0.375}Ca_{0.375}MnO_3$ and $La_{0.5}Ca_{0.5}MnO_3$: in $La_{0.5}Ca_{0.5}MnO_3$, field-induced melting of COO primarily proceeds by a gradual reduction of COO domain regions. By contrast, in $La_{0.25}Pr_{0.375}Ca_{0.375}MnO_3$, the more rapid field-induced melting of COO occurs via the enhancement of FM domain regions that are already present in the material—even at low temperatures and $H=0$ T—by Pr-substitution. However, thermal melting in $La_{0.25}Pr_{0.375}Ca_{0.375}MnO_3$ and $La_{0.5}Ca_{0.5}MnO_3$ proceeds in the same fashion, namely by disrupting COO domain regions and increasing the volume of the PM phase.

These results further suggest that Griffiths phase models[55,56,57] may be appropriate descriptions of the disordered $La_{0.25}Pr_{0.375}Ca_{0.375}MnO_3$ system. The Griffiths phase describes the behavior of a random magnetic system that is between the completely disordered and ordered magnetic phases,[56] and was first used to describe a randomly dilute Ising ferromagnet in the regime between the observed (suppressed) FM critical temperature T_C and the critical temperature T_G of the pure magnet (i.e., at which temperature the magnetization is non-analytic in an external field).[55] This suppression of the critical temperature was associated in the Griffiths phase with the effects of quenched disorder, which partition the pure system into small ferromagnetic clusters. There have been several recent studies that identify a Griffiths phase in the manganites.[57,58] In particular, we note that the T-x phase diagram of $La_{1-x}Sr_xMnO_3$ reported by Deisenhofer et al.,[58] in which a Griffiths phase regime is identified, is quite similar to the T-y phase diagram of $La_{0.625-y}Pr_yCa_{0.375}MnO_3$,[14] in which a coexistence regime of FM and CO phases having different length scales is reported. Indeed, based on this similarity, we can make a rough correspondence between the phases of $La_{1-x}Sr_xMnO_3$ and $La_{0.625-y}Pr_yCa_{0.375}MnO_3$. The correspondence between the phases observed in these materials is summarized in Table I.

Therefore, we propose that the field- and temperature-dependent behavior observed in $La_{0.25}Pr_{0.375}Ca_{0.375}MnO_3$ can be understood in the context of Griffiths physics: In this picture, T_C is dependent on the size of the ferromagnetic clusters introduced by disorder, i.e., the cluster size scales with T_C. This is consistent with our observation that the transition from COO to FM in $La_{0.25}Pr_{0.375}Ca_{0.375}MnO_3$ can be readily induced by applying even relatively weak fields at low temperatures, where larger FM regions coexist with COO regions.

Further, the abrupt field-induced transition between COO and FM phases in $La_{0.25}Pr_{0.375}Ca_{0.375}MnO_3$—which is in contrast to the more gradual transition observed in $La_{0.5}Ca_{0.5}MnO_3$—is naturally explained in this description as due to a percolation transition of the FM clusters, which can be associated with a non-analyticity of the magnetization in the Griffiths model.[57] However, we hasten to add that there has been no systematic theoretical study of the field-dependence of "Griffiths phase" systems, and more theoretical study would be welcome to check the connection between the novel field-induced melting behavior observed in $La_{0.25}Pr_{0.375}Ca_{0.375}MnO_3$ and that expected from Griffiths phase physics.

IV. SUMMARY AND CONCLUSIONS

Our detailed temperature- and magnetic-field-dependent Raman study of the phase transitions in $La_{0.5}Ca_{0.5}MnO_3$ and $La_{0.25}Pr_{0.375}Ca_{0.375}MnO_3$ allows us to provide specific details regarding the various structural phases that accompany thermal and field-induced melting of COO in these materials. In $La_{0.5}Ca_{0.5}MnO_3$, we have found that thermal melting exhibits three distinct temperature regimes: below 150 K, melting of COO occurs at the interface between large coherent COO regions ($P2_1/m$ space group), causing a reduction in the COO domain volume with increasing temperature, but maintaining the long-range coherence of COO domains. Between $150 \leq T \leq 170$ K, additional melting leads to the eventual collapse of long-range COO, and the evolution of a coexistence regime consisting of short-range COO ($P2_1/m$ space group) domains and "weakly JT distorted" ($Imma$ or $Pnma$ space group) regions. Above 170 K, COO domains are completely melted, leading to a weakly JT distorted ($Imma$ or $Pnma$ space group) regime. This temperature-dependent evolution of the spectra is suggestive of a first-order "electronic crystallization" transition in $La_{0.5}Ca_{0.5}MnO_3$, with the kinetics in the coexistence region corresponding to the propagation of a phase front. The field-induced melting process of COO in $La_{0.5}Ca_{0.5}MnO_3$ is found to be quite similar to the thermal melting process, suggesting that field-induced melting of COO in $La_{0.5}Ca_{0.5}MnO_3$ is associated with a first-order quantum phase transition: the application of a magnetic field disrupts antiferromagnetic order preferentially at the surface of COO regions, giving rise to heterogeneous melting of the coherent long-range COO regions, and a three-stage field-dependent melting process: a low-field regime in which a long-range "strongly JT distorted"/COO phase is present; an intermediate-field regime in which strongly JT distorted/COO domain regions coexist with weakly JT distorted/FMM domain regions; and finally a high-field regime in which a long-range "weakly JT distorted"/FMM phase associated with either a $Imma$ or $Pnma$ structure is present. This three-stage field-dependent melting process in $La_{0.5}Ca_{0.5}MnO_3$ is consistent with the three distinct structural phases identified by Tyson et al.[37] over a more limited temperature range. Based on our results, we were able to obtain a complete phase diagram of $La_{0.5}Ca_{0.5}MnO_3$ in the temperature range 6–170 K and in the field range 0–9 T. Notably, the similarity between thermal and field-induced melting in $La_{0.5}Ca_{0.5}MnO_3$ is reflected in critical field values, $H^*(T)$—between the long-range COO and intermediate "coexistence" regimes—and $H_c(T)$—between the intermediate "coexistence" and weakly JT distorted FMM regimes—that decrease roughly linearly with decreasing temperature at a rate of ~ -0.2 T/K. Further, our results suggest an approximate T=0 critical point of $H^*(T{=}0) \sim 30$ T for $La_{0.5}Ca_{0.5}MnO_3$, indicative of a very robust COO in

TABLE I: This table summarizes the corresponding phases among the T-x phase diagram of $\mathrm{La_{1-x}Sr_xMnO_3}$, the T-y phase diagram of $\mathrm{La_{0.625-y}Pr_yCa_{0.375}MnO_3}$, and the T-H phase diagram of $\mathrm{La_{0.25}Pr_{0.375}Ca_{0.375}MnO_3}$.

$\mathrm{La_{1-x}Sr_xMnO_3}$ [a]		$\mathrm{La_{0.625-y}Pr_yCa_{0.375}MnO_3}$ [b]		$\mathrm{La_{0.25}Pr_{0.375}Ca_{0.375}MnO_3}$ [c]
Griffiths phase	$0.075 \leq x \leq 0.16$ $T_C(x) < T < T_G$	short-range CO/FM phase	$0.275 \leq y \leq 0.40$ $T_C(y) < T < T_{CO}$	$\sim$80 K$\leq T \leq \sim$200 K 0T$< H < H_c(T)$
FM/insulating phase	$0.075 \leq x \leq 0.16$ 0K$< T < T_C(x)$	long-range CO/FM phase	$0.275 \leq y \leq 0.40$ $T_C(y) < T < T_{CO}$	0K$\leq T \leq \sim$80K 0T$< H < H_c(T)$
FM/metallic phase	$0.16 < x$ $T < T_C(x)$	long-range FM /short-range CO phase	$y < 0.275$ $T < T_C(y)$	$H_c(T) < H$

[a] Ref. 58
[b] Ref. 14
[c] From our discussion

$\mathrm{La_{0.5}Ca_{0.5}MnO_3}$.

To investigate the effects of disorder on commensurate COO in $\mathrm{La_{0.5}Ca_{0.5}MnO_3}$, we also examined the $\mathrm{La_{0.25}Pr_{0.375}Ca_{0.375}MnO_3}$ system. We found that while thermal melting in $\mathrm{La_{0.25}Pr_{0.375}Ca_{0.375}MnO_3}$ is not significantly different from that in $\mathrm{La_{0.5}Ca_{0.5}MnO_3}$, field-induced melting in $\mathrm{La_{0.25}Pr_{0.375}Ca_{0.375}MnO_3}$ differs dramatically from that in $\mathrm{La_{0.5}Ca_{0.5}MnO_3}$: the application of a magnetic field in the former material is found to induce an abrupt transition from a long-range COO to a "weakly JT distorted"/FM phase with a very narrow intermediate coexistence field regime, in contrast to a gradual transition observed in $\mathrm{La_{0.5}Ca_{0.5}MnO_3}$. Moreover, the phase diagram deduced for $\mathrm{La_{0.25}Pr_{0.375}Ca_{0.375}MnO_3}$ reveals that the critical field $H_c(T)$ between COO and weakly JT distorted regimes increases from $\sim$2 T at T=3.5 K to 4 T at T=130 K, in contrast to a linear decrease of the $H_c(T)$ with decreasing temperature in $\mathrm{La_{0.5}Ca_{0.5}MnO_3}$. This suggests that disordering COO with Pr-substitution does not appreciably affect temperature-dependent melting of COO, but does significantly affect the field-induced melting of COO. We argue that the magnetic field induced coherence between FM domains—which originate from the introduction of Pr in $\mathrm{La_{0.25}Pr_{0.375}Ca_{0.375}MnO_3}$—accelerates the disruption of antiferromagnetic order in COO, and leads to a distinctly different process of field-induced melting of COO from that observed in $\mathrm{La_{0.5}Ca_{0.5}MnO_3}$. In particular, we argue that field-induced melting of COO in $\mathrm{La_{0.5}Ca_{0.5}MnO_3}$ is best described as the percolation of FM domains introduced at H=0 T by Pr-substitution, and we suggest the Griffiths phase physics may be an appropriate theoretical model for describing the unusual temperature- and field-dependent transitions observed in $\mathrm{La_{0.25}Pr_{0.375}Ca_{0.375}MnO_3}$.

Acknowledgments

This material is based on work supported by the U.S. Department of Energy, Division of Materials Sciences, under Award No. DE-FG02-07ER46453, through the Frederick Seitz Materials Research Laboratory at the University of Illinois at Urbana-Champaign. Work at Hamburg was supported by the German funding agency under RU 773/3-1, and work at Rutgers was supported by NSF-DMR-0405682.

---

[1] P. E. Schiffer, A. P. Ramirez, W. Bao, and S.-W. Cheong, Phys. Rev. Lett. **75**, 3336 (1995).

[2] H. Kuwahara, Y. Tomioka, A. Asamitsu, Y. Moritomo, and Y. Tokura, Science **270**, 961 (1995).

[3] Y. Tomioka, A. Asamitsu, Y. Moritomo, H. Kuwahara, and Y. Tokura, Phys. Rev. Lett. **74**, 5108 (1995).

[4] A. Asamitsu, Y. Moritomo, Y. Tomioka, T. Arima, and Y. Tokura, Nature **373**, 407 (1995).

[5] H. Kawano, R. Kajimoto, M. Kubota, and H. Yoshizawa, Phys. Rev. B **53**, R14709 (1996).

[6] Y. Tomioka, A. Asamitsu, H. Kuwahara, Y. Moritomo, and Y. Tokura, Phys. Rev. B **53**, R1689 (1996).

[7] H. Y. Hwang, S.-W. Cheong, P. G. Radaelli, M. Marezio, and B. Batlogg, Phys. Rev. Lett. **75**, 914 (1995).

[8] J. Fontcuberta, B. Martínez, A. Seffar, S. Piñol, J. L. García-Munoz, and X. Obradors, Phys. Rev. Lett. **76**, 1122 (1996).

[9] P. G. Radaelli, G. Iannone, M. Marezio, H. Y. Hwang, S-W. Cheong, J. D. Jorgensen, and D. N. Argyriou, Phys. Rev. B **56**, 8265 (1997).

[10] C. N. R. Rao and A. K. Cheetham, Science **276**, 911 (1997).

[11] V. Laukhin, J. Fontcuberta, J. L. García-Munoz, and X. Obradors, Phys. Rev. B **56**, R10009 (1997).

[12] M. Fäth, S. Freisem, A. A. Menovsky, T. Tomioka, J. Aarts, and J. A. Mydosh, Science **285**, 1540 (1999).

[13] Y. Moritomo, Phys. Rev. B **60**, 10374 (1999).

[14] Uehara, S. Mori, C. H. Chen, and S.-W. Cheong, Nature **399**, 560 (1999).

[15] C. N. R. Rao, P. V. Vanitha, and Anthony K. Cheetham,

Chem, Eur. J. **9**, 828 (2003).

[16] S. Jin, T. H. Tiefel, M. McCormack, R. A. Fastnacht, R. Ramesh, and L. H. Chen, Science **264**, 413 (1994).

[17] Y. Tokura, Y. Tomioka, H. Kuwahara, A. Asamitsu, Y. Moritomo, and M. Kasai, J. Appl. Phys. **79**, 5288 (1996).

[18] A. P. Ramirez, J. Phys. Condens. Matter **9**, 8171 (1999).

[19] M. B. Salamon and M. Jaime, Rev. Mod. Phys. **73**, 583 (2001).

[20] E. O. Wollan and W. C. Koehler, Phys. Rev. **100**, 545 (1955).

[21] Z. Jirak, S. Krupicka, Z. Simsa, M. Dlouha, and Z. Vratislav, J. Magn. Magn. Mater. **53**, 153 (1985).

[22] C. N. R. Rao, Anthony Arulraj, A. K. Cheetham, and Bernard Raveau, J. Phys.: Condens. Matter **12**, R83 (2000).

[23] P. G. Radaelli, D. E. Cox, M. Marezio, S.-W. Cheong, P. E. Schiffer, and A. P. Ramirez, Phys. Rev. Lett. **75**, 4488 (1995).

[24] P. G. Radaelli, D. E. Cox, M. Marezio, and S.-W. Cheong, Phys. Rev. B **55**, 3015 (1997).

[25] J. B. Goodenough, Phys. Rev. **100**, 564 (1955).

[26] Q. Huang, J. W. Lynn, R. W. Erwin, A. Santoro, D.C. Dender, V. N. Smolyaninova, K. Ghosh, and R. L. Greene, Phys. Rev. B **61**, 8895 (2000).

[27] C. H. Chen and S.-W. Cheong, Phys. Rev. Lett. **76**, 4042 (1996).

[28] S. Mori, C. H. Chen, and S.-W. Cheong, Phys. Rev. Lett. **81**, 3972 (1998).

[29] M. V. Abrashev, J. Bäckström, L. Börjesson, M. Pissas, N. Kolev, and M. N. Iliev, Phys. Rev. B **64**, 144429 (2001).

[30] M. N. Iliev and M. V. Abrashev, J. Raman Spectrosc. **32**, 805 (2001).

[31] J. Tao and J. M. Zuo, Phys. Rev. B **69**, 180404(R) (2004).

[32] C. H. Chen, S. Mori, S-W. Cheong, Phys. Rev. Lett. **83**, 4792 (1999).

[33] Y. Okimoto, Y. Tomioka, Y. Onose, Y. Otsuka, and Y. Tokura Phys. Rev. B **59**, 7401 (1999).

[34] S. Naler, M. Rübhausen, S. Yoon, S. L. Cooper, K. H. Kim, and S. W. Cheong, Phys. Rev. B **65**, 092401 (2002).

[35] M. Roy, J. F. Mitchell, A. P. Ramirez, and P. Schiffer, Phys. Rev. B **58**, 5185 (1998).

[36] J. H. Jung, H. J. Lee, T. W. Noh, E. J. Choi, Y. Moritomo, Y. J. Wang, and X. Wei, Phys. Rev. B **62**, 481 (2000).

[37] T. A. Tyson, M. Deleon, M. Croft, V. G. Harris, C.-C. Kao, J. Kirkland, and S-W. Cheong, Phys. Rev. B **70**, 024410 (2004).

[38] S. A. Kivelson, E. Fradkin, and V. Emery, Nature **393**, 550 (1998).

[39] C. S. Snow, S. L. Cooper, G. Cao, J. E. Crow, H. Fukazawa, S. Nakatsuji, and Y. Maeno, Phys. Rev. Lett. **89**, 226401 (2002).

[40] C. S. Snow, J. F. Karpus, S. L. Cooper, T. E. Kidd, and T.-C. Chiang, Phys. Rev. Lett. **91**, 136402 (2003).

[41] J. F. Karpus, R. Gupta, H. Barath, S. L. Cooper, and G. Cao, Phys. Rev. Lett. **93**, 167205 (2004).

[42] M. N. Iliev, M. V. Abrashev, H.-G. Lee, V. N. Popov, Y. Y. Sun, C. Thomsen, R. L. Meng, and C. W. Chu, Phys Rev B **57**, 2872 (1998).

[43] K. Yamamoto, T. Kimura, T. Ishikawa, T. Katsufuji, and Y. Tokura, Phys. Rev. B **61**, 14706 (2000).

[44] E. Granado, N. O. Moreno, A. Garcia, J. A. Sanjurjo, C. Rettori, I. Torriani, S. B. Oseroff, J. J. Neumeier, K. J. McClellan, S.-W. Cheong, and Y. Tokura, Phys. Rev. B **58**, 11435 (1998).

[45] E. Liarokapis, Th. Leventouri, D. Lampakis, D. Palles, J. J. Neumeier, and D. H. Goodwin, Phys. Rev. B **60**, 12758 (1999).

[46] L. Martín-Carrón, A. de Andrés, M.J. Martínez-Lope, M.T. Casais, and J.A. Alonso, Phys. Rev. B **66**, 174303 (2002).

[47] M. V. Abrashev, V. G. Ivanov, M. N. Iliev, R. A. Chakalov, R. I. Chakalova, and C. Thomsen, Phys. Status Solidi B **215**, 631 (1999).

[48] M. V. Abrashev, J. Bäckström, L. Börjesson, V. N. Popov, R. A. Chakalov, N. Kolev, R. -L. Meng, and M. N. Iliev, Phys. Rev. B **65**, 184301 (2002).

[49] B. Nienhuis, E. K. Riedel, and M. Schick, Phys. Rev. B **23**, 6055 (1981).

[50] H. W. J. Blöte and R. H. Swendsen, Phys. Rev. Lett. **43**, 799 (1979).

[51] G. A. Baker and J. W. Essam, J. Chem. Phys. **55**, 861 (1971).

[52] D. G. Bergman and B. I. Halperin, Phys. Rev. B **13**, 2145 (1976).

[53] Y. Imry and M. Wortis, Phys. Rev. B **19**, 3580 (1979).

[54] M. Aizenman and J. Wehr, Phys. Rev. Lett. **62**, 2503 (1989).

[55] R. B. Griffiths, Phys. Rev. Lett. **23**, 17 (1969).

[56] A. J. Bray, Phys. Rev. Lett. **59**, 586 (1987).

[57] P. Y. Chan, N. Goldenfeld, and M. Salamon, Phys. Rev. Lett. **97**, 137201 (2006).

[58] J. Deisenhofer, D. Braak, H. -A. Krug von Nidda, J. Hemberger, R. M. Eremina, V. A. Ivanshin, A. M. Balbashov, G. Jug, A. Loidl, T. Kimura, and Y. Tokura, Phys. Rev. Lett. **95**, 257202 (2005).

[59] In the *Pbnm* representation, $d_{3x^2-r^2}$ and $d_{3y^2-r^2}$ orbitals alternate lying in the *a*-*b* plane.

[60] In this cross configuration of the incident and scattered light polarizations, i.e., ($\mathbf{E}_i$, $\mathbf{E}_s$)=(**L**, **R**), the A_g, B_{1g}, B_{2g}, and B_{3g} symmetries are allowed because the diagonal elements of the Raman tensor, which represent the A_g symmetry, are not equal, i.e., $\alpha_{xx}\neq\alpha_{yy}\neq\alpha_{zz}$. While all the symmetries are allowed in the ($\mathbf{E}_i$, $\mathbf{E}_s$) =(**L**, **R**) configuration, the previous observations indicate that the B_{1g} and B_{3g} symmetry modes in *Pnma* (B_{2g} and B_{3g} in *Pbnm*) are very weak,[29] so that most of the observed modes have either A_g or B_{2g} (B_{1g} in *Pbnm*) symmetry.

[61] The frequencies of stretching modes depend on the Mn-O bond length while those of bending modes depend on the *R*-O bond length in RMnO$_3$, and the Mn-O bond length doesn't significantly change depending the *R* element type but the *R*-O bond length does. See Ref. 46.

[62] This Raman activation due to the symmetry lowering is well described with the A_g JT mode in Fig 2(b). Therefore, the A_g JT mode, in fact, gives information about the symmetry lowering to $P2_1/m$ as well as the degree of JT distortions.

[63] We've already assigned the 480 cm^{-1} peak to the JT modes, and the observed frequencies, 400 cm^{-1} and 430 cm^{-1}, correspond to the frequency dependence of bending modes reported by Martín-Carrón et al.[46] The 515 cm^{-1} mode is already assigned to one of the bending modes by Abrashev et al.[48]

[64] The 480 cm^{-1} "JT mode" was better fit to the Gaussian curve than the Lorentzian curve since it's composed of two closely adjacent modes.